Qualification of innovative floating substructures for 10MW wind turbines and water depths greater than 50m

Project acronym	LIFES50+
Grant agreement	640741
	Collaborative project
Start date	2015-06-01
Duration	40 months

Deliverable D3.5 HexaFloat robot

Lead Beneficiary	Politecnico di Milano
Due date	2017-11-30
Delivery date	2018-05-16
Dissemination level	Public
Status	Final
Classification	Unrestricted
Keywords	HexaFloat Robot; offshore wind; LIFES50+; Wind tunnel testing; Wind turbine model;
Company document number	Click here to enter text.

The research leading to these results has received funding from the European Union Horizon2020 programme under the agreement H2020-LCE-2014-1-640741.

Disclaimer

The content of the publication herein is the sole responsibility of the publishers and it does not necessarily represent the views expressed by the European Commission or its services.

While the information contained in the documents is believed to be accurate, the authors(s) or any other participant in the LIFES50+ consortium make no warranty of any kind with regard to this material including, but not limited to the implied warranties of merchantability and fitness for a particular purpose.

Neither the LIFES50+ Consortium nor any of its members, their officers, employees or agents shall be responsible or liable in negligence or otherwise howsoever in respect of any inaccuracy or omission herein.

Without derogating from the generality of the foregoing neither the LIFES50+ Consortium nor any of its members, their officers, employees or agents shall be liable for any direct or indirect or consequential loss or damage caused by or arising from any information advice or inaccuracy or omission herein.

Document information

Version	Date	Description
0.1	2018-03-21	First draft Prepared by Ilmas Bayati, Francesco La Mura Reviewed by Ilmas Bayati, Marco Belloli, Hermes Giberti Approved by Marco Belloli
0.2	2018-03-22	Draft for peer-review Prepared by Ilmas Bayati, Francesco La Mura Reviewed by Kolja Muller Approved by Marco Belloli
version	2018-05-13	Final version for QA before submission Prepared by Ilmas Bayati Reviewed by Jan Arthur Norbeck Approved by Petter Andreas Berthelsen
		In order to enter a new version row, copy the above and paste into left most cell.

Authors	Organization
Ilmas Bayati	Politecnico di Milano
Marco Belloli	Politecnico di Milano

Contributors	Organization
Hermes Giberti	Politecnico di Milano
Francesco La Mura	Politecnico di Milano

Definitions & Abbreviations

6 DoF	Six-degree-of-freedom
6-PUS	Prismatic Universal Spherical
6-RUS	Resonant Ultrasound Spectroscopy
6-UPS	Ultraviolet Photoelectron Spectroscopy
ADAMS	Automated Dynamic Analysis of Mechanical Systems
FEM	Finite Element Method
FK	Forward Kinematics
HIL	Hardware-In-the-Loop
JFMD	Jacobian-Free Monotonic-Descendent
HMI	Human-Machine-Interface
MGNR	Modified-Global-Newton-Raphson
NR	Newton-Raphson
P	Prismatic joint
PKM	Parallel kinematic machine
RMS	Root Mean Square
TCP	Tool Centre Point
U	Universal joint

Executive Summary

This report describes the design process, the realization and verification of the 6-DoF setup designed for wind tunnel hybrid tests of floating offshore wind turbines. This setup consists in a parallel kinematic robot, “HexaFloat”, designed and developed by the authors of this report, to test the dynamics of floating offshore wind turbine concepts, selected within LIFES50+ project, at the Politecnico di Milano wind tunnel, through a hybrid methodology which combines, in real-time, measurements (i.e. aerodynamic forces on the wind turbine scale model) and computations (i.e. hydrodynamic forces on the wind turbine platform). This represents the complementary test approach, with respect to the one developed at the SINTEF Ocean basin.

In particular, the different chapters give the following information:

- Geometric optimization
- Actuation chain sizing
- Mechanical design and sizing
- Control architecture and electronics

Contents

1 Introduction

Scale model testing of floating structures is a common practice in the research and developments of new concepts and systems, as it helps in driving the design choices and rapidly answers the scientific questions through a cost-effective and controlled experimental environment. Nevertheless, when the effects of wind and wave loads become comparable, model testing is affected by scaling issues (e.g. Froude-Reynolds scaling conflict) about the ability of reproducing physically the wind and wave in a proper manner. For this reason, hybrid testing both in ocean basin [1], as well as in the wind tunnel [2] seem to represent the most effective approach to relax the scaling constraints as well to exploit separately already existing wind or wave generating different facilities, instead of setting up combined tests with the mentioned problems.

In this report, the hardware/software setup for wind tunnel tests is reported, proving an overview of the design process and methodology, the development of the mechanical components, the overall control scheme, as well as a brief description of the validation procedure. More specifically, this setup consists in a 6 degree-of-freedom robot, "HexaFloat", designed to move the base of the tower of a wind turbine's scale model (e.g. 1/75 of the 10 MW DTU reference wind turbine, [3]), based on the combined effect of aerodynamic loading (i.e. measurements by means of a load balance at the base of the tower/robot's end effector) and hydrodynamic loading (i.e. real-time hydro-structure computations). The technical aspects of wind tunnel hybrid testing methodology are beyond of the scope of the present report, however, they can be found in [4] [5] [6] [7].

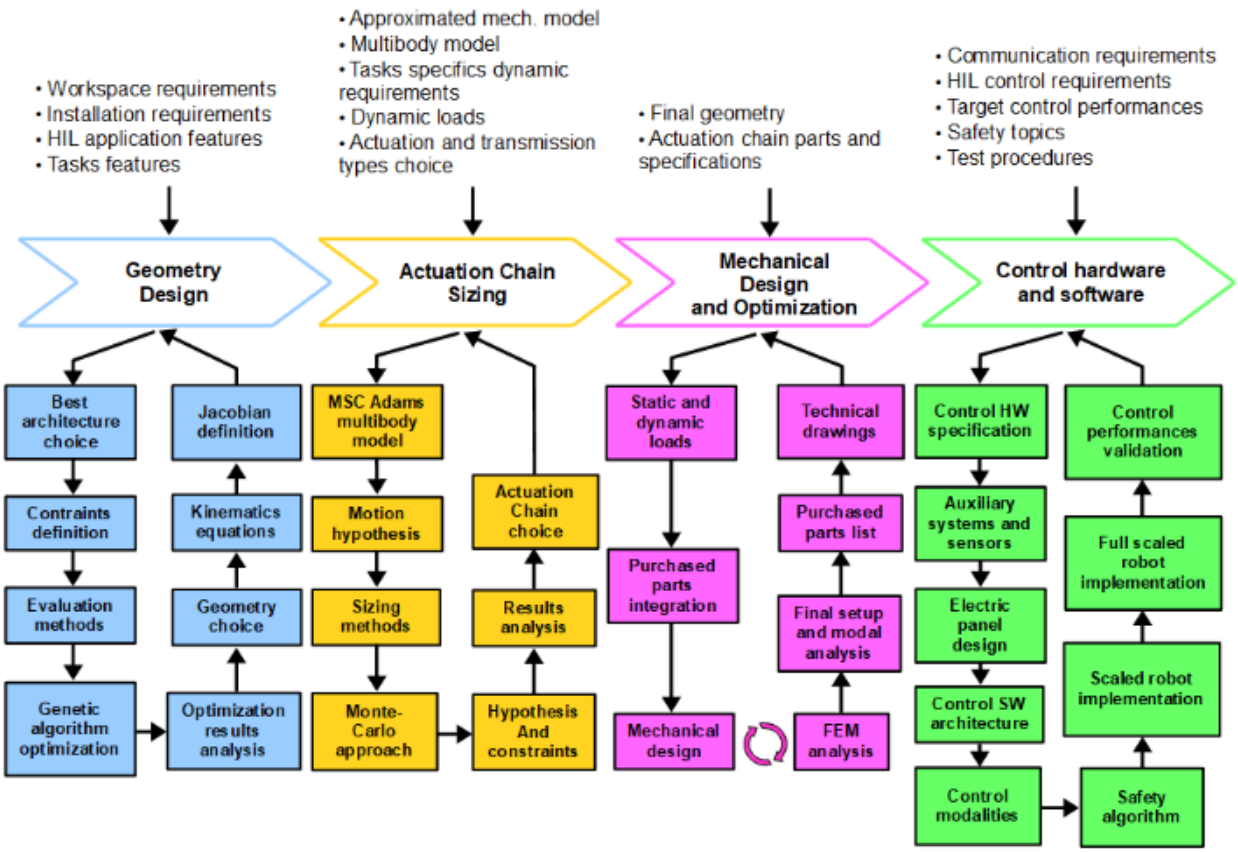

Figure 1.1 General scheme of the HexaFloat design process

In Figure 1.1 a general scheme of the design of such setup is briefly reported and it is thoroughly explained in the following chapters.

2 Geometric optimization

2.1 Choice of the architecture

Among all the possible architectures of a 6DoFs manipulators, parallel kinematic machines (PKMs) were preferred with respect to serial kinematic manipulators due to their high precision and accuracy in the end-effector positioning, high stiffness and dynamic performances.
In the first stage of the design process the main focus has to be given to the choice of the kinematic topology and the geometric dimensions [8] [9].
The most successful architectures are the 6-UPS, 6-RUS and 6-PUS.

- The 6-UPS manipulators have a kinematic chain characterised by a sequence of a universal joint at the base (U), an actuated prismatic joint (P) that varies the link's length and a spherical joint (S) connected at the mobile platform.
- The 6-RUS manipulators are characterized by fixed length links, moved by actuated revolute joints (R) located in correspondence of the base. The other joints in the kinematic chain are: an intermediate universal joint and a spherical joint connected to the mobile platform.
- The 6-PUS manipulators have again links of fixed length. The actuated prismatic joint is in general composed by a slider which moves along a rectilinear guide. The link is connected to the slider by means of a universal joint and to the mobile platform by means of a spherical joint.

The 6-PUS joints configuration has limited moving masses due to completely ground installed actuation, and greater workspace vs machine encumbrance ratio. This topology was selected in order to guarantee high performances both in terms of dynamic response and structural properties while keeping limited dimensions.
Within this category, two manipulators have been chosen as suitable candidates [10]: the Hexaglide, with 6 guides which are all parallel to each other, and the Hexaslide, whose guides are organized in 3 couples, parallel each other, arranged in radial fashion. The two manipulators have some substantial differences:

- The Hexaglide have the guides disposed all parallel to each other, which allows to have a predominant direction of motion and it is characterized by symmetry with respect to the longitudinal median plane.
- The Hexaslide is characterized by a radial symmetry with respect to the vertical axis. This characteristic leads to a greater isotropy of the workspace.

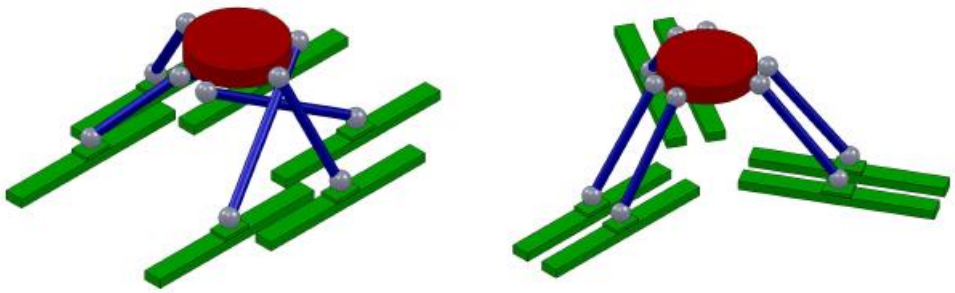

(a) Hexaglide (b) Hexaslide

Figure 2.1: Hexaglide and Hexaslide architecture

2.2 Kinetostatic optimization

Given the vertical dimensions of the wind tunnel and the height of the turbine scale model, no commercial robots on the market have been found that satisfy such a low amount of space requirement while keeping the desired workspace dimensions.
An optimization process [10] is required to synthesize the geometric parameters of the two possible robot architectures: Hexaslide and Hexaglide. In order to properly set up the process, it is first necessary to identify the geometric parameters characterizing the two architectures, then a function that mathematically describes the goal to be achieved. Finally, a set of physical constraints affecting the system have to be identified and defined in mathematical form in order to create the numeric boundaries for the solution.

2.2.1 Robot Parametrization

When choosing the number of parameters to be optimized, a trade-off needs to be considered: if the number of parameters used to characterize a machine is increased, the whole process of optimization would benefit allowing a higher freedom, however the complexity of the machine dramatically increases. Thus, a compromise needs to be found between global performances and structural modularity, which is critical in order to simplify design and optimization steps.

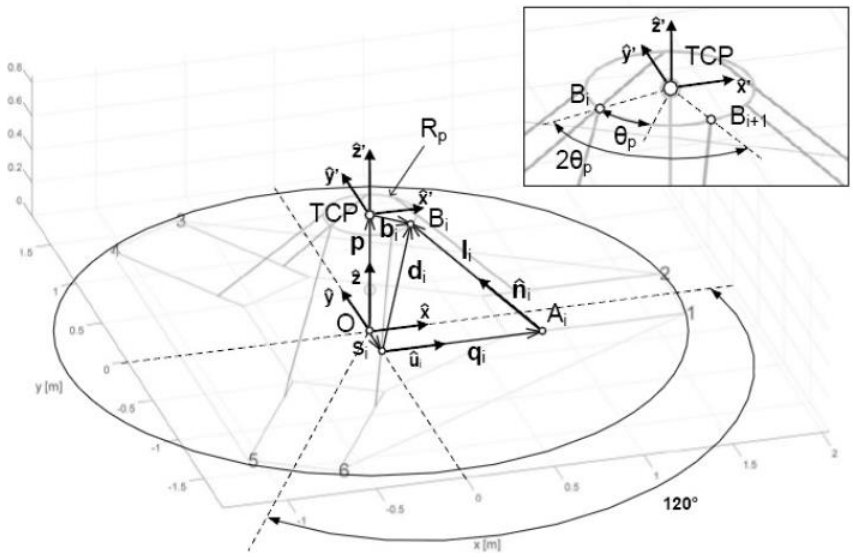

Figure 2.2: Hexaslide geometric parameters

The Hexaslide architecture can be investigated considering the following parameters for the optimization process:

- s: semi-distance between two parallel guides
- l_i: length of the links
- R_p: radius of the circumference on which the platform joints centres are located.
- θ_p: semi-angular aperture between the two segments connecting the origin of the TCP (Tool Centre Point) reference frame and a couple of platform joints.
- $z_{w\,sd}$: height of the centre of the desired workspace.

For this architecture, the same kinematic chain is replicated identically six times.

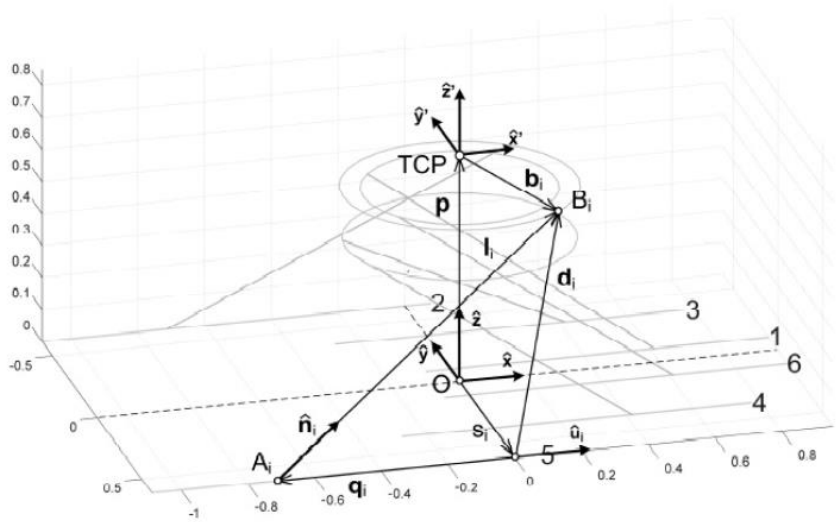

Figure 2.3: Hexaglide geometric parameters

The Hexaglide architecture can be investigated considering a higher number of parameters because three different kinematic chains can be identified in the robot configuration. The parameters to be optimized are:

- $R_{p,1}$: radius of the circumference on which the platform joints 1 and 2 are located.
- $R_{p,2}$: radius of the circumference on which the platform joints 3 and 4 are located.
- $R_{p,3}$: radius of the circumference on which the platform joints 5 and 6 are located.
- $\theta_{p,1}$: semi-angular aperture between the two segments connecting the origin of the TCP reference frame and platform joints 1 and 2.
- $\theta_{p,2}$: semi-angular aperture between the two segments connecting the origin of the TCP reference frame and platform joints 3 and 4.
- $\theta_{p,3}$: semi-angular aperture between the two segments connecting the origin of the TCP reference frame and platform joints 5 and 6.
- t_1: vertical distance between TCP and the plane where platform joints 1 and 2 lie.
- t_2: vertical distance between TCP and the plane where platform joints 3 and 4 lie.
- t_3: vertical distance between TCP and the plane where platform joints 5 and 6 lie.
- l_1: length of links 1 and 2.
- l_2: length of links 3 and 4.
- l_3: length of links 5 and 6.
- s_1: semi-distance between parallel guides 1 and 2.
- s_2: semi-distance between parallel guides 3 and 4.
- s_3: semi-distance between parallel guides 5 and 6.
- $z_{w\,sd}$: height of the centre of the desired workspace.

For this architecture, each kinematic chain is replicated twice, one on both side of the longitudinal median plain of symmetry.

2.2.2 Objective definition

The goal to be achieved is to optimize robot performances while ensuring the desired workspace boundaries. The portion of the desired workspace that the robot is not able to reach is a good candidate for the objective function to be minimized but its definition is challenging.
To define a proper objective function, the desired workspace is discretized in elementary volumes: for each elementary volume, the specific set of parameters under analysis must allow to reach its centre point. Moreover, for each centre point analysed, the resulting machine must be able to orientate the

TCP with any possible combination of pitch, roll and jaw angles varying inside a predefined range. If that is not the case, the elementary volume is added to the total volume the current set of parameters is not able to cover. To make the computational cost affordable, the three angular ranges are discretized, thus restricting the checks to a finite amount of angles combinations. The evaluation of the objective-function is performed by first fixing the mobile-platform orientation $\emptyset_m = [\alpha_m; \beta_m; \gamma_m]$, and computing the portion of volume the end-effector is not able to reach for this specific orientation as:

$$v_{nc}(\emptyset_m) = \sum_i \sum_j \sum_k c_{i,j,k}(\emptyset_m)\Delta v \qquad \begin{cases} i = 1, \dots, N_x \\ j = 1, \dots, N_y \\ k = 1, \dots, N_z \end{cases}$$

where the combination of parameters i, j, k uniquely identifies a check-point of the workspace in which N_x, N_y, N_z represent the number of discretization points, respectively along x, y, z axes. The variable $c_{i,j,k}(\emptyset_m)$ is equal to 1 if the specific parameters prevent the end-effector from reaching the pose defined by i, j, k and $\emptyset_m$, and 0 otherwise. The term Δv is the elementary volume resulting from the discretization of the workspace.
This procedure is repeated for all combinations of pitch, roll and jaw angles and the resulting value for the objective-function V_{nc} is computed as:

$$V_{nc} = \sum_m v_{nc}(\emptyset_m)$$

Even if a volume portion is discarded just for one specific orientation, that portion of workspace is excluded for the corresponding geometrical configuration. In the ideal case in which a set of parameters allows the robot to reach any point in the workspace regardless of its orientation, the objective-function would be equal to 0. On the other end, if the set of parameters doesn't allow to reach a point of the workspace, the objective-function would assume a value equal to the dimension of the single discrete volume times the number of orientations for which that volume has been discarded.

2.2.3 Constraint

The kinematic capability of reaching each point with every possible orientation is not sufficient by itself: the robot must guarantee a certain level of performances and safety, so additional constraints definition is required.

The **kinematic constraints** are defined in this way:

- Distance between the i-th platform joint and the corresponding base joint should not overcome the length of the link for geometric congruence.
- Each actuated joint coordinate must be comprised in a range defined by the dimension of the machine, since actuators stroke range have a direct impact on the major encumbrance direction of the machine, longitudinal for the Hexaglide, radial for the Hexaslide.
- Each passive joint, both platform and base ones, should respect its mobility range.

The **kinetostatic constraints** are defined by the transmission ratio between forces and moments acting on the end-effector and the actuation forces. This transmission ratio for each actuator is computed and the maximum one should be lower than a prescribed limit value. As common for PKMs, this transmission ratio varies considerably inside the nominal workspace due to non-linear kinematics, especially nearby of singular configuration, specific point in the workspace where the robot loses its ability to move the end effector in some direction.

The **geometric constraints** enforce the respect of the minimum distance between two links and between a link and the mobile platform to avoid problem of self-collision of the component for particular poses.

2.2.4 Genetic algorithm

The chosen algorithm is a single objective genetic algorithm [11]. A genetic algorithm approaches the problem by using the principles of natural selection.
At first, several solutions, each of which is an *individual* and whose collection is a *population*, are created by selecting randomly the parameters from their predefined ranges. Each individual of the population is evaluated, and its performance is judged on the base of the defined cost function. From this population, the worst individuals are discarded while the fittest group concurs at creating a new population by three different mechanisms: a small elite group is replicated unchanged, thus transmitting all their genes; a fixed percentage of new individuals is obtained by combining parameters (genes) of the best for the previous population using a crossover rule; the remaining part of individuals is generated by randomly mutating one or more genes of previous non discarded individuals. As in real life, this type of continuous adaptation creates a very robust organism. The whole process continues through many generations, with the best genes being transmitted to future generations and more and more efficient combination of genes being developed through every generation.

The use of a semi-stochastic search and the evaluation of the performances of different individuals at each iteration, simplify the process of finding the global minimum of the objective-function to be minimized. The steps characterizing this kind of algorithm are:

- Choice of a sufficiently high number of individuals representing a generation to have a significant statistical sample.
- Evaluation of the performances for every one of the current generation depending on the values assumed by its genes.
- Choice of the group with better performances that will constitute the elite and that will pass unchanged to the next generation.
- Creation of a new generation based on elite's choice, crossover and mutation.
- Performance computation of the new generation individuals and comparison with the desired goal.

The algorithm would keep modifying parameters trying to cover the desired workspace as much as possible and minimizing the defined objective function.

2.2.5 Optimization Process Results

The following reports the lower and upper bounds imposed at the beginning of the optimization and the optimal values obtained.

Symbol	*Lower Bound*	*Upper Bound*	Optimal value	MU
z_{WSd}	400	500	463.6	mm
s	200	300	203.1	mm
l	400	700	686.6	mm
R_p	200	250	238.7	mm
θ_p	0	60	38.5	$^\circ$

Table 2.1: Limits and results of the Hexaslide optimization

Symbol	*Lower Bound*	*Upper Bound*	Optimal value	MU
z_{wsd}	500	700	593.9	mm
s_1	100	980	1050.8	mm
s_2	100	980	277.7	mm
s_3	100	980	330.2	mm
l_1	600	1600	1207.7	mm
l_2	600	1600	873.9	mm
l_3	600	1600	825.7	mm
$R_{p,1}$	200	400	306.2	mm
$R_{p,2}$	200	400	326.7	mm
$R_{p,3}$	200	400	275.9	mm
t_1	-200	0	-183.0	mm
t_2	-200	0	-72.4	mm
t_3	-200	0	-22.9	mm
θ_{p_1}	10	170	77.3	$^\circ$
θ_{p_2}	10	170	37.9	$^\circ$
θ_{p_3}	10	170	100.6	$^\circ$

Table 2.2: Limits and results of the Hexaglide optimization

Minimum distance between the links, minimum distance between links and platform, transmission ratio and maximum and minimum strokes of the actuated joint coordinates are obtained through optimization process. The results are mapped all over the workspace to guide in the choice of the best architecture, the one with better performances in all the workspace points. The following conclusions hold:

1. Hexaslide:
    a. Schematics: both the height and the surface encumbrance of the manipulator are quite limited. When the robot is in the home position the links are arranged in such a way that a good compromise is achieved between the capabilities of producing velocity in every direction and bearing external forces without too much actuators effort.
    b. Link-to-link and link-to-platform minimum distances: The link-to-platform minimum distance recorded is greater than 270mm all over the workspace, thus avoiding any risk of collision between the legs.
    c. Force transmission ratio: the worst case shown by the computation is near the limit value of 5 but only in few small lower regions of the workspace.
    d. Actuated joints maximum and minimum stroke: since the joints coordinate distance with respect to the global reference frame is always positive, it's sufficient to check the maximum value to evaluate the encumbrance of the robot. This joint coordinate excursion is about 1m.

2. Hexaglide:
    a. Schematics: The surface encumbrance of the second robot is much higher with respect to the Hexaslide. In addition, the centre of the desired workspace in the optimized configuration is positioned at a higher quote compared with the Hexaslide result.
    b. Link-to-link and link-to-platform minimum distances: no risk of self-collision between the elements is detected.
    c. Force transmission ratio: the transmission ratio remains limited above 2.5
    d. Maximum and minimum stroke: encumbrance results higher with respect to the Hexaglide configuration.

It can be concluded that Hexaslide architecture is more compact with respect to Hexaglide but reaches higher values of the forces transmission ratio. The Hexaslide architecture has been chosen due to its lower vertical encumbrance, more compact surface dimensions, better workspace isotropy and lower position of the workspace centre. All these features make it possible to install the machine underneath the wind tunnel floor level, reducing the robot`s influence on the air flow quality and keeping the turbine farther from the wind tunnel ceiling. Moreover, Hexaslide offers two more advantages: all the elements that constitute the links are the same for the 6 kinematic chains and the radial symmetry simplifies the design process. From now on the machine will be referred as Hexafloat, while the term Hexaslide will refer to the specific architecture of the robot.

2.3 Kinematics

Inverse and forward kinematics has been studied to completely define the non-linear geometric equations that link workspace degrees of freedom to actuated joint space.

2.3.1 Inverse kinematics

In order to study Inverse Kinematics, two different reference frames have been considered, the global one and the local one with origin in the TCP and in-built with the robot platform. With reference to Figure 2.3, two different vector closures for each kinematic chain can be set up to compute the joint coordinates vector q.

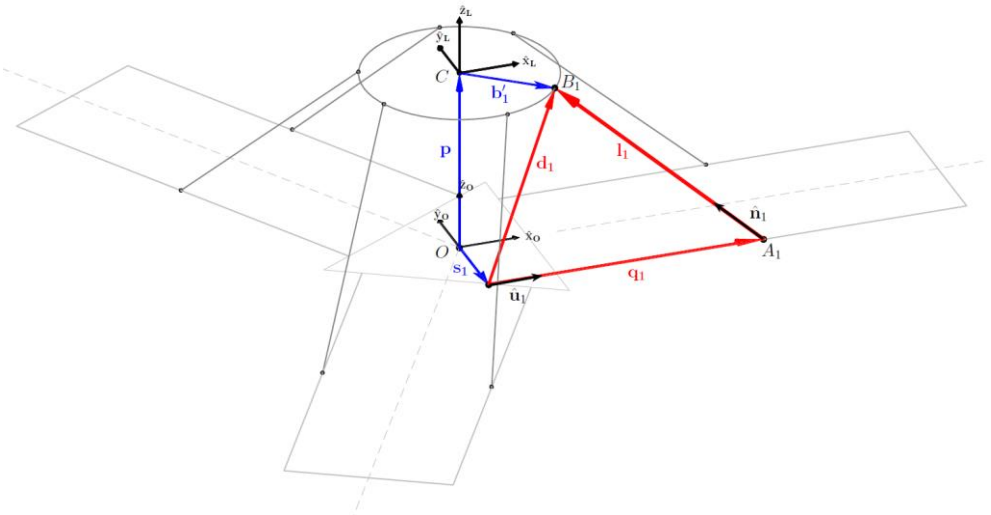

Figure 2.4: Vector closures used to solve the IK problem: in blue the 1st closure while in red the 2nd one.

The first vector closure allows determination of the absolute position vector $\mathbf{d}_i$ of the platform joint B_i with respect to a point which is the intersection of $\mathbf{q}_i$ direction with its orthogonal plane passing through the global origin. Each $\mathbf{s}_i$ has fixed length with different orientation in the absolute X_o-Y_0 plane.

$$\boldsymbol{d}_i = \boldsymbol{p} + R_{TCP}\boldsymbol{b}_i - \boldsymbol{s}_i$$

Where R_{TCP} is the rotation matrix defining the platform's orientation. This matrix is used to transform the expression of $\mathbf{b}_i$, constant in a rotating local reference frame, in its equivalent with respect to a zero-orientation local frame translating with the platform. Position vector $\mathbf{p}$ and the offset $\mathbf{s}_i$ complete the transformation from the zero-orientation local frame to the global one**.**
The second vector closure allows determination of the position of the i-th slider on the guide.

$$\boldsymbol{l}_i = \boldsymbol{d}_i - \boldsymbol{q}_i\hat{u}_i$$

The magnitude of $\mathbf{l_i}$ vector corresponds to the length of the robot leg while $\hat{u}$ is representing the guide direction unitary vector.
This procedure is identical, except for the orientation of $\mathbf{b_i}$, $\hat{u}_i$ and $\mathbf{s_i}$, for all the six links of the robot.

2.3.2 Forward Kinematics

The Hexafloat robot is not equipped with sensors able to directly measure the platform position and orientation, therefore a good quality FK could work as a virtual sensor for the pose of the robot. A high frequency estimation of the actual pose of the TCP could be a valuable feedback tool for the other controller in the HIL (Hardware In the Loop) setup. Small calculation time and overall stability, in case of numerical algorithms, is nevertheless crucial.
Extensive researches have been made to find out analytical methods to solve the FK of PKMs, especially for Gough-Steward configuration, but the pose of the robot has not been expressed in an explicit form so far.
Considering numerical methods, Newton-Raphson (NR) algorithm has its numerical stability highly dependent on the accuracy of the initial approximation of the solution vector so a monotonic descent operator can be added obtaining the so called Modified-Global-Newton-Raphson (MGNR) algorithm, able to estimate the FK solution of 6 DoFs parallel robots for any initial guess in the non-singular workspace without divergence.
The algorithm requires the definition of a system of six non-linear equations and the evaluation of a matrix of partial derivatives.

$$\underline{f_i}(\underline{x}) = \underline{0}$$

$$P_{ij} = \frac{\partial f_i}{\partial x_j}$$

The evaluation of partial derivatives matrix can be simplified by implementing Jacobian-Free-Monotonic-Descendent (JFMD) algorithm. A first-order Taylor expansion can be used to approximate the partial derivatives matrix in a numerical way.
The JFMD method is implemented through the following steps:

- proper initial guess x_0 for the solution is chosen and the corresponding $\underline{f}(\underline{x}) = \underline{0}$ is calculated;
- the (k + 1)[th] solution attempt is calculated according to this formula:

$$x_{k+1} = x_k - \rho_k [J(x_k)]^{-1} f(x_k)$$

  where ρ_k ($0 \leq \rho_k \leq 1$) is the monotonic descent factor. It starts from 1 and during each iteration is calculated as $\rho_k = 2^{-m}$ where m is the number of rechecking times in the corresponding iteration, necessary to obtain the monotonic trend.
  The approximated Jacobian matrix is evaluated from the first-order Taylor expansion of its partial derivatives and considering a perturbation parameter η of 1e-16. The i-th row and j-th column of the approximated Jacobian matrix is evaluated as:

$$J_{ij} = \frac{f_i(x + \eta_j e_j) - f_i(x)}{\eta_j}$$

- convergence criterion is defined imposing the error to satisfy the following inequality:

$$\left|\left| f\left(x_k - \rho_k [J(x_k)]^{-1} f(x_k)\right) \right|\right|_2 \leq ||f(x_k)||_2$$

- the algorithm stops if convergence is achieved or the maximum number of iterations is reached:

$$||f(x_{k+1})||_2 \leq \delta = 1e-10 \qquad or \qquad k \geq k_{max} = 20$$

where δ is the required computation tolerance and k_{max} is the given maximum number of iterations.

The first initial guess is taken near Home Position, where the robot is supposed to be when switched on. For the following times, the initial guess is chosen as the estimated pose at the previous cycle. The logic of the JFMD algorithm is clarify in the flow chart in Figure 2.5. Thanks to C language implementation, this routine can converge to a solution in few iteration, with a mean calculation time of around 50us. This performance allows the use of FK as a virtual real time sensor with sufficient accuracy.

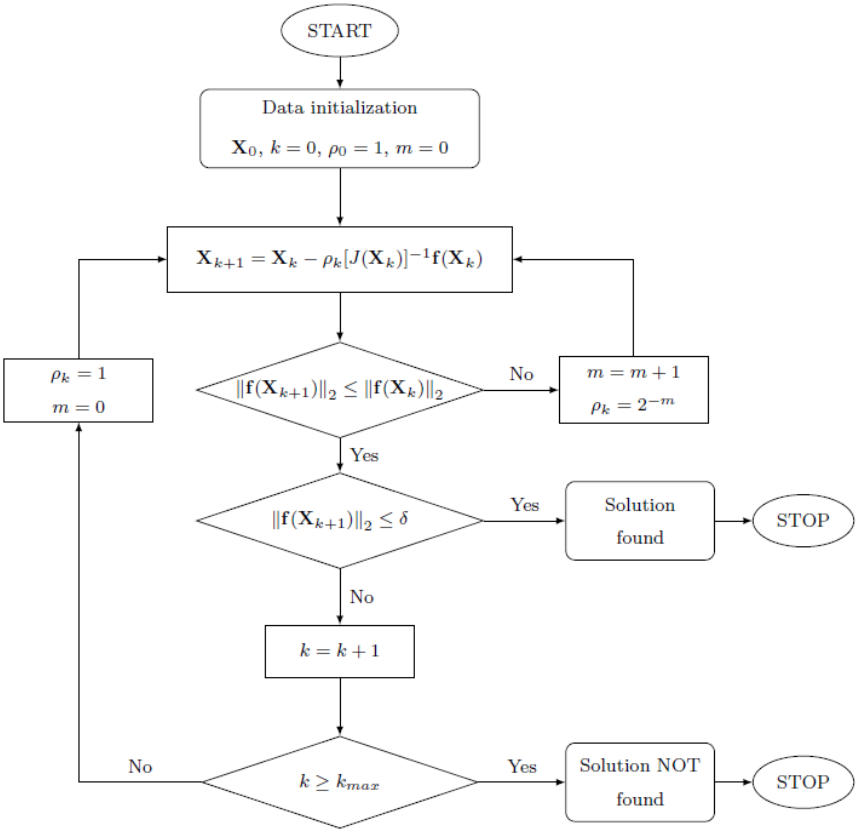

Figure 2.5: Flow chart of the JFMD algorithm

2.3.3 Velocity analysis and kinetostatic

To determine the relation between the velocity of the TCP and the ones of the joint coordinates, it is necessary to calculate the Jacobian matrix. If all the six links are considered together, a compact matrixial form coupling the joint velocity vector $\dot{q}$ and the workspace velocity vector w can be defined.

$$\begin{bmatrix} \hat{n}_1^T\hat{u}_1 & \cdots & 0 \\ \vdots & \ddots & \vdots \\ 0 & \cdots & \hat{n}_6^T\hat{u}_6 \end{bmatrix}\dot{q} - \begin{bmatrix} \hat{n}_1^T & \cdots & (b_1\times\hat{n}_1)^T \\ \vdots & \ddots & \vdots \\ \hat{n}_6^T & \cdots & (b_6\times\hat{n}_6)^T \end{bmatrix} w = 0$$

$$[J_q]\,\dot{q} - [J_{gs}]^{-1} w = 0$$

and with some algebraic passages:

$$\dot{q} = [J]^{-1} w$$

The solution of the kinetostatic analysis provides the actuation forces τ_a required to balance the external forces f_{ec} applied to the TCP. Thanks to the virtual work principle and knowing that the virtual variation of the workspace coordinates is related to the virtual variation of the joint coordinates through the Jacobian matrix $[J]$ the actuation forces can be computed as:

$$\tau_a = -[J]^T f_{ec}$$

The representation of the way in which forces applied to the robot platform are transmitted to the actuators is done considering the unitary hypersphere of forces in the workspace. This unitary hypersphere is transformed into a hyper-ellipsoid in the space of actuation forces. This representation is not realistic, and it assumes that if one of the forces applied to the TCP reaches the maximum value of 1, the other components must be null. A better representation is provided considering a hyper-cube of unitary semi-side that is transformed into a hyper-polyhedron through the Jacobian matrix.

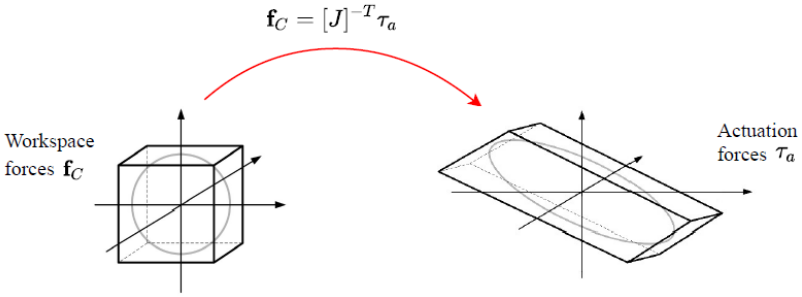

Figure 2.6: Transformation of the workspace forces unitary hyper-cube into the actuation forces hyper-polyhedron

It should be noticed that the inverse Jacobian matrix can be split into a translational and a rotational part. The rotational components of the inverse Jacobian matrix are dimensional since they correspond to a length. To let all the elements of the inverse Jacobian matrix be dimensionless, it is useful to divide the rotational components by a scale factor defined as characteristic length L_c. In this way a normalized inverse Jacobian matrix is obtained, and it's used to obtain the maximum actuation force.

3 Actuation chain sizing

3.1 Multibody model

A multibody model of the robot has been developed in ADAMS to compute those dynamic and kinematic quantities that allow to properly size mechanical components as well as the actuating system [12]. The inertial properties of all elements are not known, for this reason, an iterative process is required, where a first estimation of the inertial properties of all components is used to derive a first multibody model. The results obtained from the simulations performed on this model are then used to design the mechanical components of the robot and once all elements are defined, the multibody model is updated with the new masses and inertial properties and the simulations are performed again in order to check that the newly computed quantities remain close to those obtained in the first set of simulations.

3.1.1 Reference frames and parametrization

The first step in creating the model is the definition of a set reference frames located in position that allows to easily define inertial properties, joints, applied forces, measurements points. The reference frames created are listed below:

- TCP reference frame
- Six reference frames denoted with B_i in correspondence of the centre of the end-effector joints
- Six reference frames denoted with A_i in correspondence of the centre of the base universal joints
- Six reference frames denoted P_i located at the origin of the guides axes

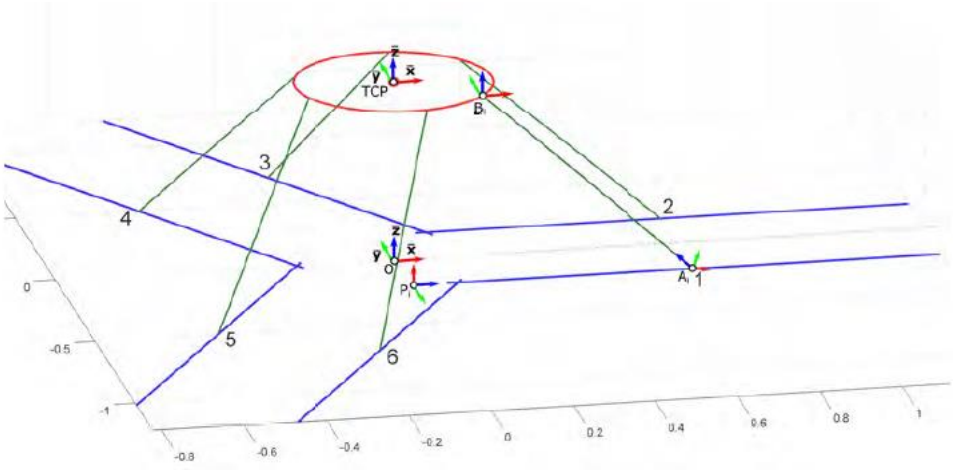

Figure 3.1: reference frames configuration

3.1.2 Modelling of bodies and constraints

Three main components for each kinematic chain can be identified:

- Platform: it considers the platform itself, the six spherical joints attached to it, the six axes load cell used to compute the forces and moments exerted by the turbine scale model on the robot. Due to the symmetry the centre of mass is expected to be located on the z axis of the TCP reference frame and principal axes of inertia are expected to be parallel to the axes of the TCP.
- Links: they can be represented as cylinders whose centre of mass is in the middle of the link and whose principal axes of inertia are aligned with those of the A_i reference frame.
- Sliders: they take into account universal joints, joints support and carriage of the transmission unit. Since these bodies will be subjected to a purely translational motion during simulations, it is sufficient to recover just their total mass.

The schematization with the equivalent mass and inertial properties of the assembly is possible because the model described in this section is supposed to be rigid.

Spherical, Universal and Prismatic joints are formalized by using two reference frames for each joint, each of them rigidly linked to one of the body connected by the joint: the mechanical and geometrical features of each joint are respected by limiting the relative motion between these two reference frames, both locking one or more relative degrees of freedom and giving limited range of displacement/rotation for those allowed.

3.2 Sizing tools

A proper sizing of mechanical components and actuating system requires the knowledge of the most power demanding motion the machine is required to execute, considering both the motion law features and the influence of robot dynamics and carried inertias. The trajectory the robot is required to follow is not known in advance and so it could be necessary to analyse any combination of a set of parameters that fully characterize the motion of the end-effector. The deterministic procedure designed is the following:

1. Partition of the workspace in a finite number of portions
2. For each point determine the admissible range of motion parameters for each degree of freedom: these ranges must be discretized in order to obtain a finite number of combinations.
3. Generation of the time histories of the 6 DoFs of the end-effector.
1. Solution of the IK problem to find the corresponding joint coordinates time histories.
2. Solution of the inverse dynamics problem for all possible cases.

3.2.1 End-effector motion characterization

The time history of the sea level ε can be expressed as:

$$\varepsilon(t) = \rho(t)\cos(\omega t + \varphi(t))$$

Where ρ is the amplitude, ω the pulsation, and φ the phase shift. Both amplitude and phase shift change very slowly in time, so it is reasonable to assume they are constant for the whole duration of the simulation and the time history of each DoF is described as:

$$j(t) = A_{0,j} + A_j \cos(2\pi f_j t + \varphi_j) \quad with \quad j = x, y, z, \alpha, \beta, \gamma$$

Where $A_{0,j}$is an offset parameter considering the initial pose of the robot.

These equations describe only the regular wave condition, even though the experimental test will be conducted both with regular and irregular waves generation. The worst operating condition may be represented by the case in which all frequencies f_j and amplitudes A_j assume their maximum value. However, besides not being physically meaningful and representative of reality, the intrinsically non-linear kinematics of the robot may invalidate this assumption. As a matter of fact, it is not guaranteed that this is the most demanding case in terms of internal loads, motor torques, velocities and accelerations. Furthermore, a simple co-sinusoidal motion of the end-effector is translated into a periodic motion of the joint coordinates where higher order harmonics with respect to the f_j appear. It is difficult to predict if the energy associated with the higher order harmonics of a specific f_j is bigger than the energy of the harmonics corresponding to a lower f_j.

The four characteristic parameters are so defined in the following ranges:

- Initial pose $A_{0,j}$: may vary in the range $\pm L_{W\,Sd,j}$
- Frequency f_j: in the range between f_{min} and f_{max}
- Phase shift φ_j: in the range of [0, 2 π]
- Amplitude A_j: its maximum range is $[-L_{W\,Sd,j}, L_{W\,Sd,j}]$ and the relation $|A_{0,j} \pm A_j| \leq L_{W\,Sd,j}$ has to be verified to guarantee that the end-effector remains within the boundaries of the desired workspace. The effective range of A_j is obtained by combining the maximum range with the expressed relation, eventually modifying it if $A_{0,i}$ is different than zero.

3.2.2 Monte-Carlo Method

Due to the described difficulties during the identification of the most demanding combination of motions, a statistical approach had been designed, based on the Monte-Carlo Method.

This novel approach is implemented as follows:

1. Choice of a sufficiently high number M of simulations, each of which has a specified time history for every DoF.
2. Definition of the Probability Density Functions of the input parameters that define every motion law: it is assumed that at the initial instant the TCP may be located with the same probability in any point of the workspace. The PDF chosen for the parameters describing the motion are:
    a. Initial pose: Uniform distribution
    b. Frequency: Uniform distribution
    c. Phase shift: Uniform distribution
    d. Amplitude: Rayleigh distribution
3. Repeated sampling of the chosen PDFs: each parameter is assigned a random value for each simulation. The result is a set of M vectors fully defining a 6-DoF motion law to be assigned to the TCP.

4. Solution of the IK problem to find the joint coordinates time histories q(t) to be used as inputs for the simulations involving the multibody model.
5. Solution of the inverse dynamics problem for each of the M simulations
6. Post-processing: evaluation of a distribution among the M simulations of the parameters of interest.

3.2.3 Post-processing

The sizing of the mechanical components requires that the following quantities are computed:

- Slider velocities
- Slider accelerations
- Forces exerted by the motors on the sliders
- Axial forces along the guide
- Load factor

A set of condensed values is required to easily compare these quantities with the corresponding limit values specified by the manufacturers. These condensed values are computed with the following procedure:

1. Extraction of maximum values recorded for each simulation
2. Among the M maximum values obtained, the highest value is computed.
3. The range between 0 and the highest value computed is divided in a prescribed number of intervals.
4. For each interval, the number of occurrences of the M values that fall within the limits of the interval itself is computed.

A set of discrete PDFs is obtained, and it represents the probability that the maximum value recorded during a simulation is comprised within a certain interval.

Parameter		Value
$\dot{q}_{max}$	Maximum slider velocity	1,67 m/s
$\ddot{q}_{max}$	Maximum slider acceleration	28,52 m/s^2
$F_{trac\ link\ max}$	Maximum link traction force	1127,43 N
$F_{comp\ link\ max}$	Maximum link compression force	1385,78 N
$F_{m,max}$	Maximum guide axial load	1188,20 N
β	Load factor	32 881,39 W/s

Table 3.1: Maximum values of the parameters

3.3 Actuating system sizing procedure

A proper selection of the actuating system requires sizing both the electric motor and the transmission unit. To achieve a correct choice of motor and transmission, it is necessary to verify the following relations [13]:

- Limit on maximum torque:

$$\max|C_m(t)| < C_{m,max} \quad and \quad \max|C_m(t)| < C_{t,max}$$

- Limits on nominal torque:

$$C^*_{m,rms} < C_{m,nom}$$

- Limit on maximum speed:

$$\max|\omega_r(t)| < \tau\omega_{m,max} \quad and \quad \max|\omega_r(t)| < \omega_{t,max}$$

Being $C_m$the motor torque, $C_{m,max}$ the maximum torque the motor can generate, $C_{t,max}$ the maximum torque the transmission unit is able to bear. As well ω_r represents the resistant speed computed on the load side, $\omega_{m,max}$ is the maximum speed the motor can reach without damaging its mechanical components, $\omega_{t,max}$ is the maximum speed the slider can achieve without damaging mechanical components.
From the power balance and the thermal check inequality it is possible to determine the transmission ratio.

$$\alpha > \beta + \left[C^*_{r,rms}\left(\frac{\tau_{rid}}{\sqrt{J_m}}\right) - \dot{\omega}_{r,rms}\left(\frac{\sqrt{J_m}}{\tau_{rid}}\right)\right]^2$$

where the acceleration factor α and the load factor β are defined as:

$$\alpha = \frac{C^2_{m,nom}}{J_m}$$
$$\beta = 2\left[\dot{\omega}_{r,rms}C^*_{r,rms} + (\dot{\omega}_r C^*_r)_{mean}\right]$$

The RMS values of torque and acceleration are defined as:

$$C^*_{r,rms} = \sqrt{\frac{1}{t_c}\int_0^{t_c}[C^*_r(t)]^2 dt} \qquad and \quad \dot{\omega}_{r,rms} = \sqrt{\frac{1}{t_c}\int_0^{t_c}[\dot{\omega}_r(t)]^2 dt}$$

The acceleration factor α is a property of the motor alone, so it is possible to compute it directly from datasheets. The load factor β instead, depends only on the specific results obtained from the multibody simulations.
As a first test, the optimal transmission ratio value τ opt is identified. This value could find no matching from the motor transmissions available on the market, so it is necessary to find two solutions that specify a range of acceptable values for the transmission ratios.
As this range is defined, it is necessary to compute the limit transmission value of the working cycle and check its value to be sure the motor is able to perform the working cycle.

$$\tau_{lim} = \frac{\max|\omega_r(t)|}{\omega_{m,max}}$$

$$\max(\tau_{lim}, \tau_{min}) < \tau < \tau_{max}$$

The results obtained from the simulations refer to the forces and linear accelerations to be applied to the sliders to achieve the desired end-effector motion. Equivalent torque and angular acceleration required to the motor are evaluated as follows:

$$\dot{\omega}_{r,i} = \frac{\ddot{q}_i(t)}{\tau_{TU}} \qquad C_{robot,i}(t) = \tau_{TU}F_{robot,Xi}(t)$$

Given the high velocity requirements, the use of a reducer would be counterproductive. A direct coupling between the motors and the guides has been realized and so a unitary value of τ_{red} is imposed.
Heat dissipation check was executed on different OMRON motors and further checks were performed on maximum torque required.
Due to the requirements of high dynamic performances, stiffness and precision of the whole machine, a recirculating ball screw was chosen as linear actuation system. The double carts configuration, characterized by a couple of runners per guide, was selected to guarantee a more uniform load distribution.
Main checks consider are: the installed ball-screw lead, the total length of the system, the maximum

allowed velocities and the forces that the guide could bear. The following table reports the checked parameters to establish if the guide was acceptable or not.

Parameter	Value		Limit value	UoM
Length of the guide	1100	$>$	650	mm
Max Velocity	1.67	$<$	2.66	m/s
Max Acceleration	28.5	$<$	50	m/s^2
F_x	1385	$<$	12250	N
F_y	1385	$<$	69600	N
F_z	1385	$<$	69600	N
M_x	174	$<$	3028	Nm
M_y	174	$<$	2290	Nm
M_z	174	$<$	2290	Nm

Table 3.2: Summary of checks done on guides

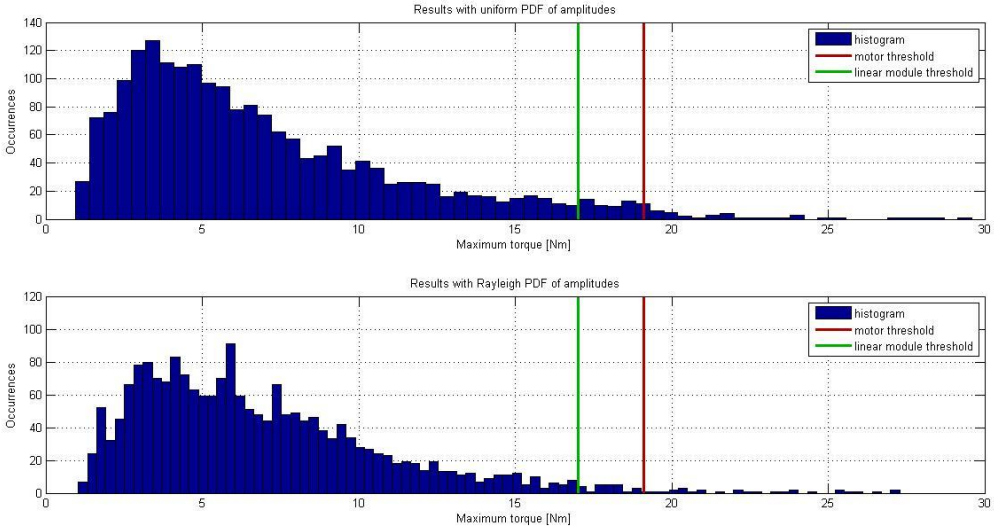

Figure 3.2: Maximum torque distribution along all the simulations

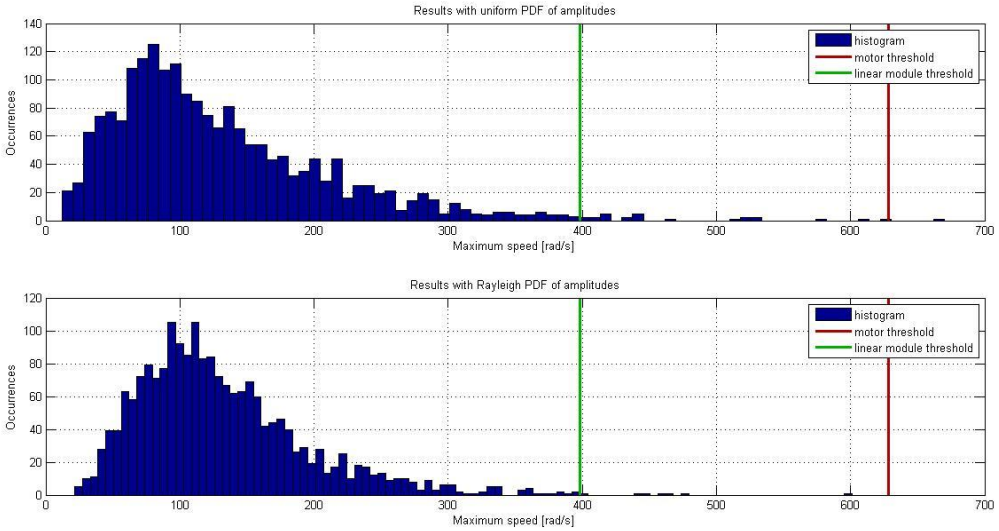

Figure 3.3: Maximum angular velocity distribution along all the simulations

4 Mechanical design and sizing

The design process followed is iterative: preliminary models that satisfy the required parameters previously computed were firstly created, then each part was refined and improved to enhance its characteristics and to reduce the mass and the realization costs.
The multibody model is used with the purpose of performing dynamic analyses that are then post processed in order to be used in the sizing of the mechanical components and of the actuating system.

4.1 Static analysis

From dynamic analysis performed the most critical load acting on links is evaluated. For the sake of safeness, an overestimated value of 2500N is adopted as design value in the static model, both in traction and compression. This choice has been done considering the results obtained from dynamic simulations, from which the most critical load acting on link was 1385N. The software adopted for this kind of model is Autodesk Inventor Professional 2015 because it allows good coherence in the results compared with software developed for this type of analysis and a quick update of the model when geometrical modifications occur. In the optimization process, several models have been developed involving different assemblies or individual parts. Considering the final configuration selected, fig. 4.11, the following considerations hold:

- Part on ground: The symmetry of the assembly allows modelling only one third of it. Only the aluminium profile of the linear actuator is modelled because it is the component supporting the vertical loads. On each guide, a vertical load of 2500N (worse case) is applied and positioned at combinations of 0%, 25%, 50%, 75%, 100% of the total actual stroke of the sliders. Local stresses and displacements never exceed critical values as shown in fig. 4.1.
- Joint: bearings have been substituted with infinitely rigid components to preserve all the components coupling. Different configurations of angle are tested both in compression and traction with an applied load of 2500N. As reported in fig. 4.2 and 4.3, only the rod presents visible deformations and stresses. To better investigate the behaviour of internal components, other analyses have been carried out and no problems have been highlighted by the results:
    - Inner Block: a load of 2500N is split in two equal loads each one acting on a bearing set. Maximum stress registered is 85MPa which is much below the admissible stress of 250MPa, fig. 4.4.
    - Support shaft: a load of 1250N is applied for simulating the presence of two Support blocks per Joint. The test is made by loading one end of the shaft and maintaining the other one fixed. Results are shown in fig. 4.5.
    - Inner shaft: a load of 2500N is applied in the mid-span and both ends are pinned to simulate the presence of the two bearings. Results are reported in fig. 4.6.
- Link: an axial load of 2500N is applied and only traction and compression have been tested. Bearings are substituted with rigid parts. Relevant stresses are registered on the upper and lower rod, but their values are much below the critical one, as show in fig. 4.7, 4.8, 4.9.
- Platform: two horizontal forces are applied at different heights over the TCP. The first of 100N located at 1,0m and the second of 50N at 1,5m correspond respectively to inertial load and aerodynamic thrust calculated by the wind tunnel working team. To obtain a safer design, these loads are doubled, and two additional loads were applied at the same heights of the previous ones but in an orthogonal direction. These loads have a magnitude which is one half of the previous ones. As in fig. 4.10, loads of this magnitude are borne very well by the structure both in terms of stresses and displacements.
- Lifting system: a configuration that would allow a total lift of 150mm in a time of about 15 seconds with a cycloidal motion law is achieved. The usage of the lifting system allows having both robot links and motors unloaded during the whole stroke. This avoids the components to overcome the critical load zones and start working only when loads are plenty below their limits. Furthermore, the robot must overcome a singularity when moving from Home Position to the

configuration in which it is placed under the wind tunnel floor and vice versa. The lifting system helps to overcome this singularity configuration both in the rise and return phase. The analysis reveals maximum load occurrence at the initial phase of the rise and FEM analysis assures that stresses stay below the critical values.

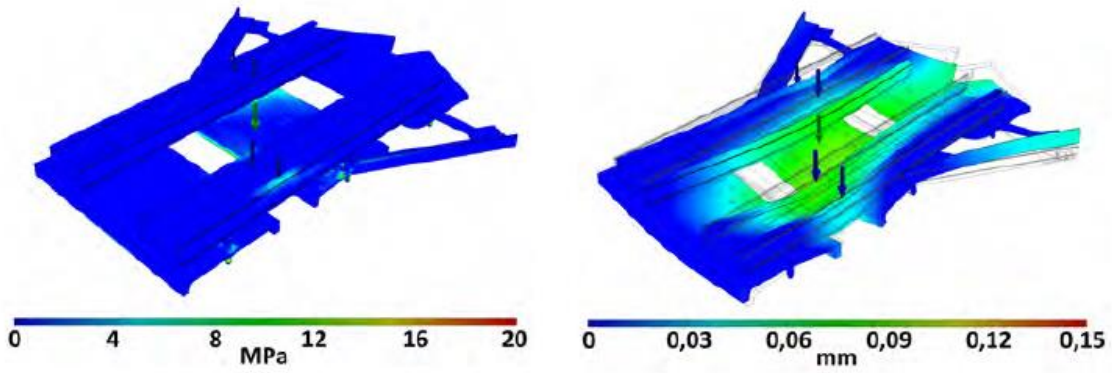

(a) *Von Mises stresses* (b) *Displacements*

Figure 4.1: Parts on ground static analysis

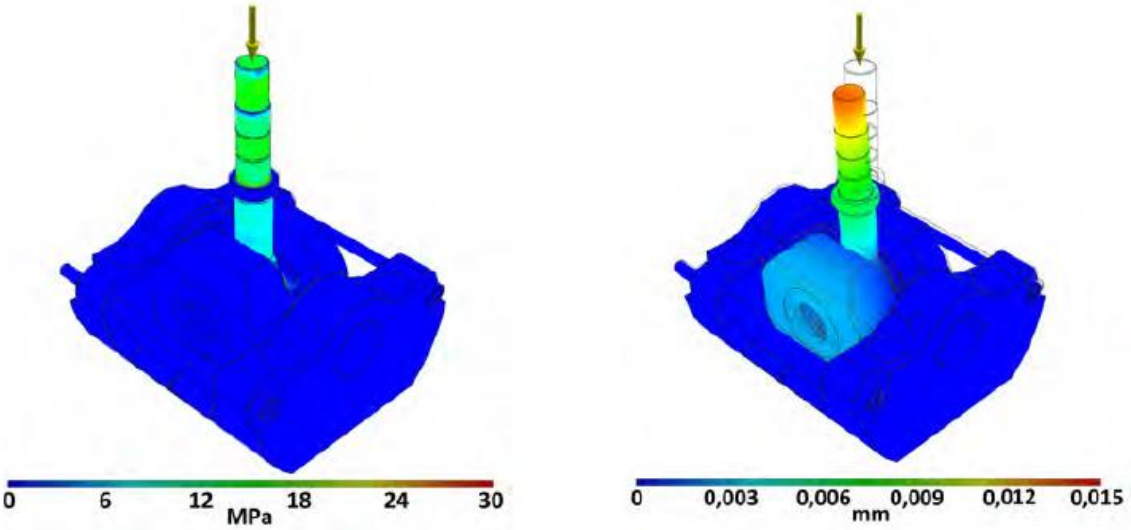

(a) *Von Mises stresses* (b) *Displacements*

Figure 4.2: Joint static analysis

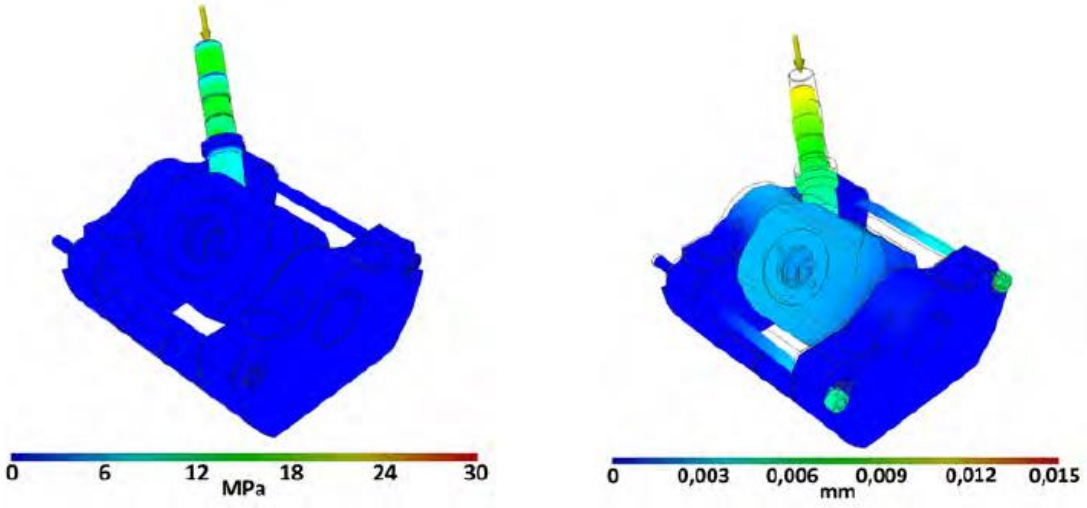

(a) *Von Mises stresses* (b) *Displacements*

Figure 4.3: Joint static analysis, inclined configuration

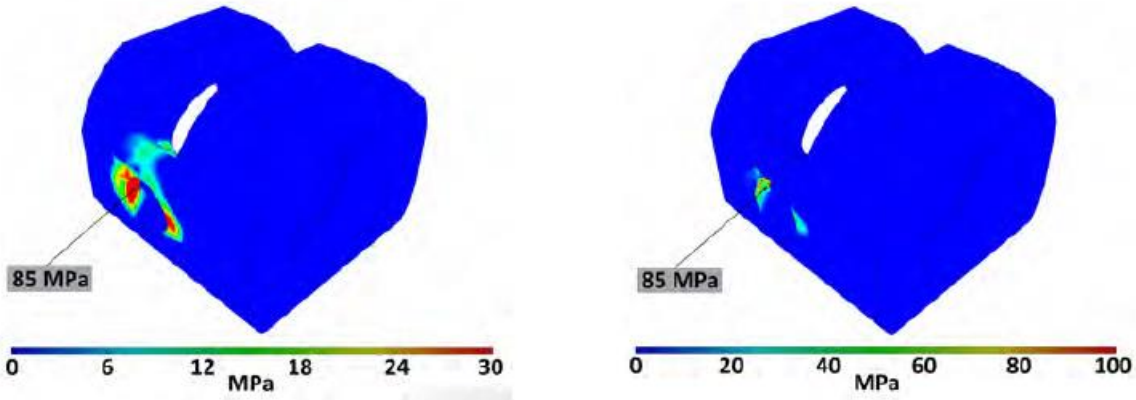

(a) *Von Mises stresses with full scale of* 30 MPa (b) *Von Mises stresses with full scale of* 100 MPa

Figure 4.4: Inner block static analysis

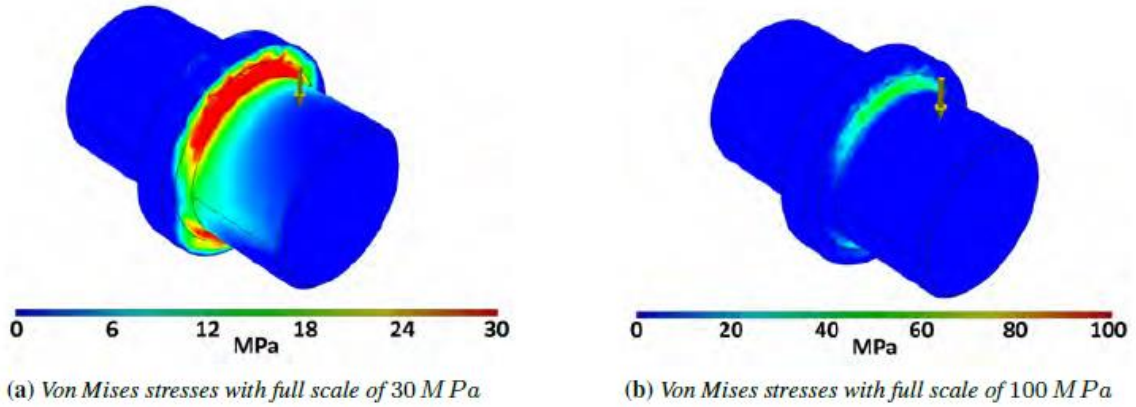

(a) *Von Mises stresses with full scale of* 30 MPa (b) *Von Mises stresses with full scale of* 100 MPa

Figure 4.5: Support shaft static analysis

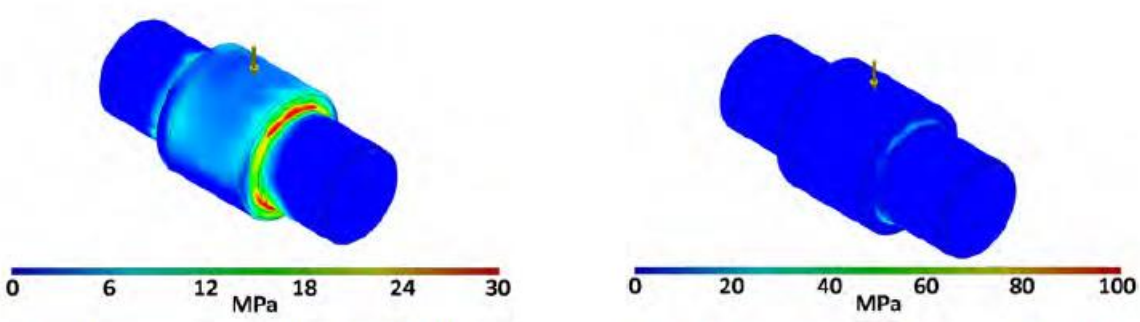

(a) *Von Mises stresses with full scale of* 30 MPa (b) *Von Mises stresses with full scale of* 100 MPa

Figure 4.6: Inner shaft static analysis

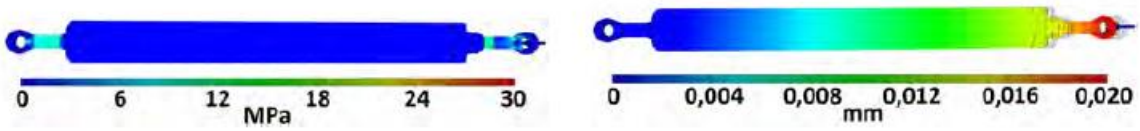

(a) *Von Mises stresses* (b) *Displacements*

Figure 4.7: Link static analysis

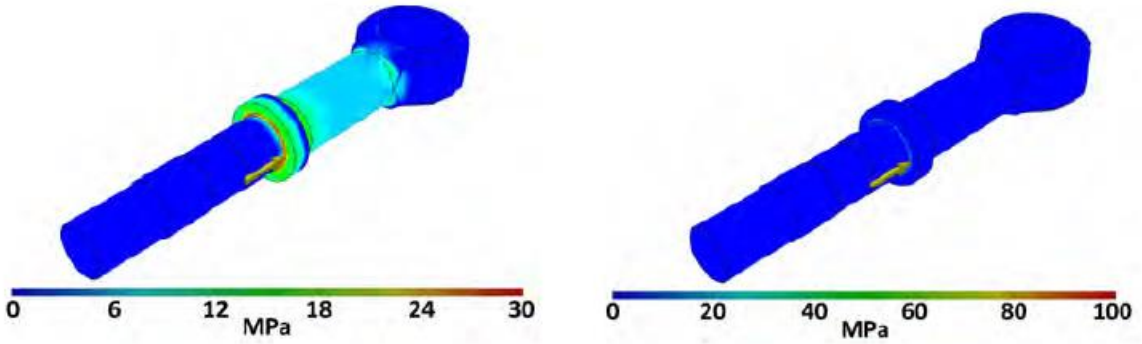

(a) *Von Mises stresses with full scale of* 30 MPa (b) *Von Mises stresses with full scale of* 100 MPa

Figure 4.8: Lower rod compression analysis

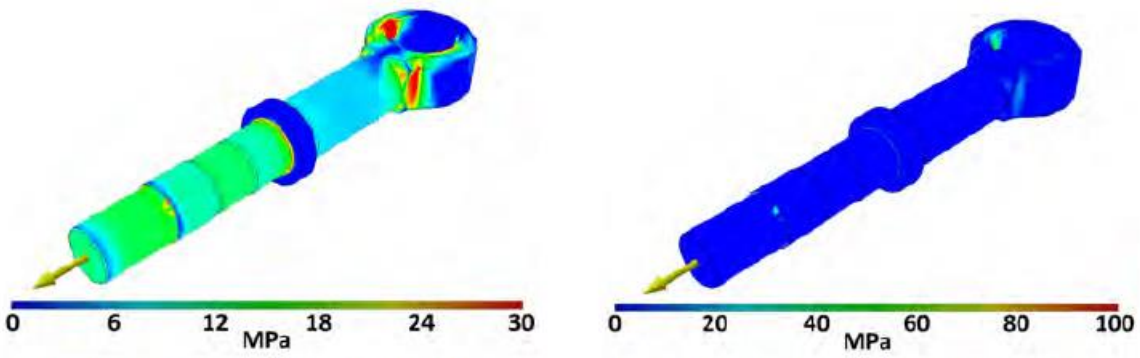

(a) *Von Mises stresses with full scale of* 30 MPa (b) *Von Mises stresses with full scale of* 100 MPa

Figure 4.9: Lower rod traction analysis

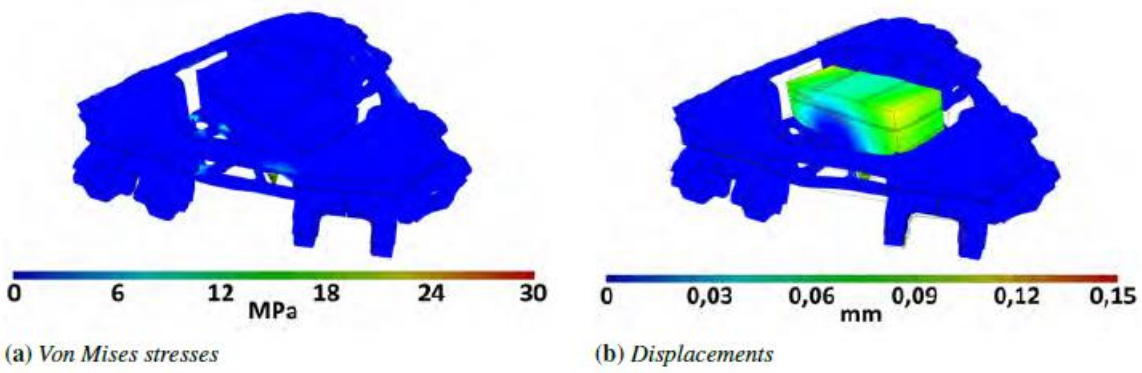

(a) *Von Mises stresses* (b) *Displacements*

Figure 4.10: Platform static analysis

4.2 Components overview

The whole machine, show in fig. 4.11, can be divided in two main parts: the actual Hexafloat robot and the auxiliary systems. In the Hexafloat robot is possible to recognise four main assemblies:

- *Parts on ground*, it is the fixed supporting structure and it holds the power and actuation units;
- *Joints*, they release and bear the moving parts providing DoFs;
- *Links*, they sustain the upper parts of the machine distancing them from the ground and providing the remaining DoFs;
- *Platform*, it is the upper part of the machine.

While the auxiliary systems include:

- *Lifting system*, it is a tool that allows to switch the machine between work and rest configurations;
- *Energy chain*, it houses cables that must be delivered to the moving platform;
- *External Sensors* used as hardware end-stroke and as zero reference for the actuators.

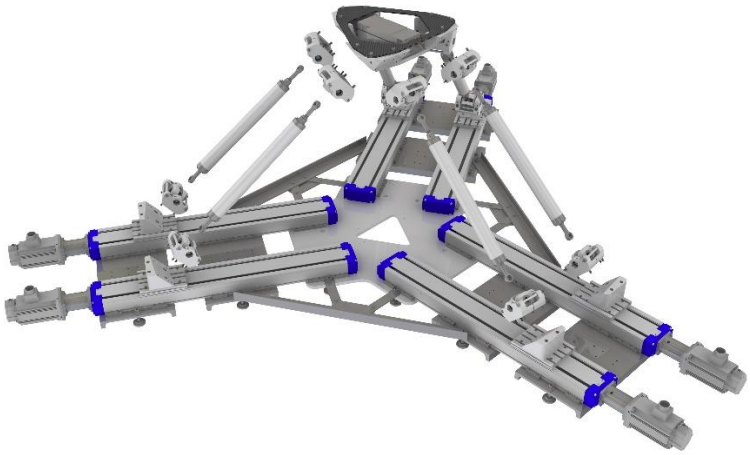

Figure 4.11: Hexafloat exploded

4.3 Parts on ground

This assembly is the framework and is the main contributor to the mass of the machine, it has the task to supply stability to the moving parts and provide the motion through the linear guides. For this reason, this assembly must be rigid to sustain static and dynamic loads.

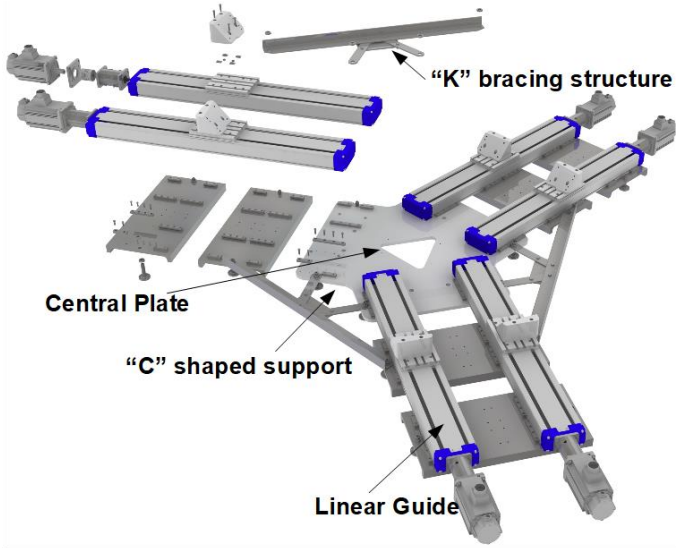

Figure 4.12: Parts on ground, partially exploded view

The central plate, made of aluminium, is mainly used to guarantee the correct orientation and position of the linear guides through calibrated recesses and to provide stiffness to the structure.
The linear actuators are grouped two by two and each couple has a relative angle of 120 degrees. This leads to a radial symmetry of the machine. Each couple of linear actuators is fixed to the Central plate. To provide further stiffness to the system, to avoid undesired tilting and relative displacement between the two couple of guides, three "K" bracing structures connect the Central plate with the internal "C" shaped supports.
Aluminium joints holder is used to couple the joints with the linear actuators. From the optimization process and solving enclosure equation when the robot is in Home Position, the direction of each link of the machine is identified and the joints holder shape and inclination is defined. The whole framework will be placed in the wind tunnel using 22 levelling elements to distribute the weight in a more uniform way and to have the guides in the same plane, without misalignment.

4.4 Joints

Joint configuration is made by an actuated prismatic joint followed by a double revolute one (universal) and a spherical one mounted on the platform.
Disposing a universal joint and a revolute one so that the rotation axis of the latter passes through the intersection of the universal joint rotation axes, it is possible to obtain the same DoFs as with a spherical joint. Therefore, the same universal joint, used in the lower part of the kinematic chain, are mounted on the platform, and the revolute ones are incorporated in the links.
Since almost all the universal joints found on the market are mainly designed to transmit torques and have not the needed precision, it was decided to design them with customized characteristics. The main feature of such joint is the possibility to have a cone shaped motion range with a semi-angle aperture of 45 degrees around the normal direction, while being designed and assembled to have zero backlash.

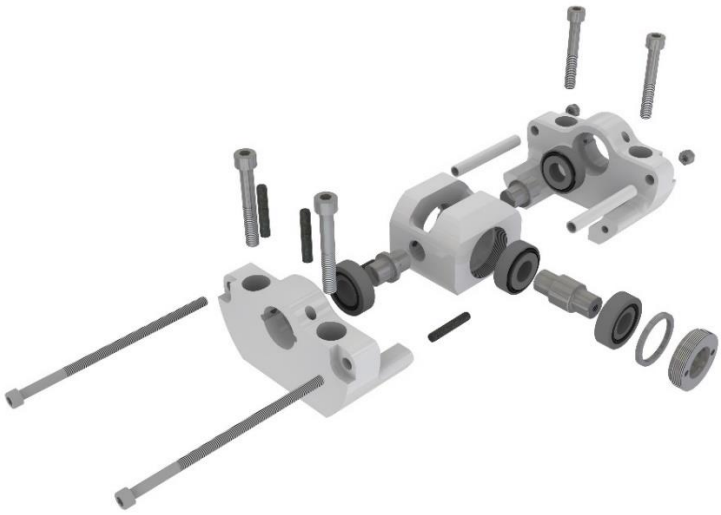

Figure 4.13: Joint exploded view

Each joint is composed by a couple of half shells connected to an inner block through two roller bearings and two support shafts, these components are tightened together by two screws and aligned by two calibrated dowel pins. In this way, the Inner block has a relative movement with respect to the shell. The further DoF is provided by other two roller bearings that sustain the inner shaft pinned to the link. All these inner components are packed through the distance ring and the closing ring. Half shells and the inner block are made of aluminium, while other components are made of steel.
The joint is fixed to the joints holder through four screws and aligned with two calibrated dowel pins.

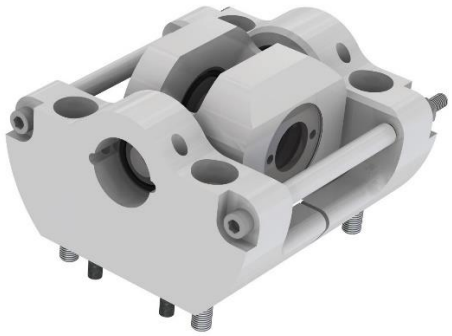

Figure 4.14: Joint assembly

4.5 Links

The Links have the task to sustain the mass of: platform, RUAG load cell, scaled wind turbine and sensors. Furthermore, the Links must provide the DoF lost when the spherical joint was substituted with the universal one.

Figure 4.15: Link exploded view

The link is composed of the following:

- *Lower rod*, made of steel, at one side it is directly connected to the Inner shaft of the Joint assembled on the Parts on ground, the other side is used to close in pack the bearings block between a shoulder and nuts;
- *Bearing case*, made of steel, it houses the bearings that provide the rotational DoF along the Link axis, and is connected to the Leg pipe through six recessed screws;
- *Leg pipe*, made of aluminium, it is a hollow cylinder with the final result of weight reduction;

- *Distance washer*, made of steel, it allows the regulation of the total Link length through a threaded connection with the Upper rod. It is even connected to the Leg pipe through six recessed screws;
- *Upper rod*, made of steel, it is the final component connected to the Inner shaft of the Joint assembled on the Platform;

4.6 Platform

The Platform must satisfy two main design parameters that result from the optimization process: the platform joint centres radius R_p and the half angle between two contiguous platform joints θ_p. The Platform is composed of:

- *Bottom plate*, made of aluminium, it has the task to sustain and distribute the load and it is the frame of the Platform;
- *Three Angular joints holder*, made of aluminium, they have the task to guarantee the correct orientation angle of the Joints when the machine is in Home Position;
- *Top plate*, made of carbon fibres, it has the task to give further rigidity to the structure;
- *RUAG 6-axis load cell*, it has the task to measure loads exchanged between the machine and the wind turbine.

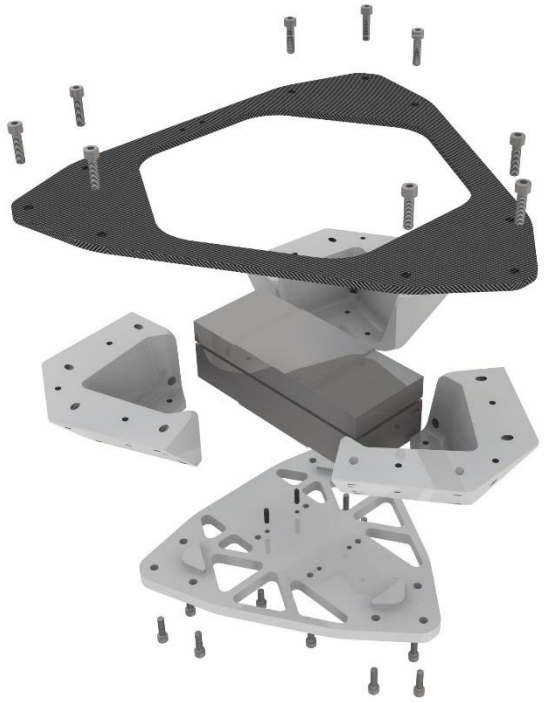

Figure 4.16: Platform exploded view

4.7 Auxiliary system: lifting system

Two auxiliary systems have been designed, a Lifting system and an Energy chain.
The Hexafloat machine is designed to be placed under the floor of the wind tunnel when it is not operative. In this configuration, the machine has to overcome a singularity to reach Home Position and the Lifting system helps the Hexafloat robot to pass this critical point in the rise and return phases.
The necessity to have a reduced vertical encumbrance of the Lifting system is given by the small available space under the floating floor. The system can be schematically modelled as in Figure 4.17 as an isosceles three-hinged arc, in which the hinge A is placed on ground, B on the Moving carriage and C at the middle part of the Three points beam, thus allowing a vertical movement of the Three points beam top end (point D). Furthermore, a four-links mechanism is coupled to this system to keep the Coupling platform mounted on the top of the lifting mechanism parallel to the ground along the whole stroke.

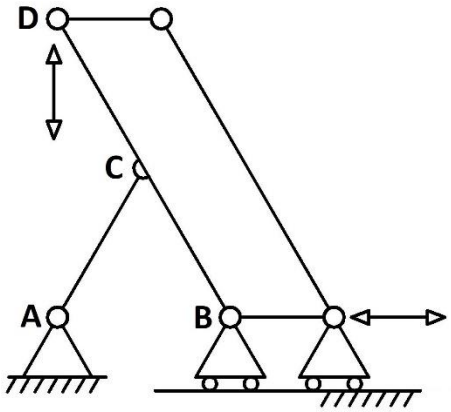

Figure 4.17: Lifting system scheme

The Moving carriage is driven by the motor through a trapezoidal screw, which converts motion from angular to linear.

Figure 4.18: Lifting system assembly

4.8 Auxiliary system: energy chain

Measuring and actuation devices will be mounted on the platform and on-board the wind turbine, these instruments need to be supplied by electric energy and they must be connected to a controller to guarantee a real time data exchange.
Therefore, a cable housing system is needed to protect cables, maintaining a good flexibility while following the platform movements, without interfering with them.

Figure 4.19: Energy chain assembly

The system is made by the following elements:

- four “L” plates support, made of steel;
- two Lateral connecting plates made of aluminium;
- two mounting brackets with strain relief mounted respectively on the Platform and on Parts on ground;
- an intermediate mounting bracket;
- a mounting sliding bracket;
- the flexible chain;

4.9 Scaled robot

A scaled version of the robot was initially produced by means of 3-D printing. This low-cost version preserves all the characteristics of the real scale robot but with some differences in the components:

- Base: it is constituted by a centring base with three sockets where three equal positioning plates are located for the guides fixing. The assembly is done by means of four M8 screws for each positioning plate and two shoulders for the correct positioning of the parts themselves. The positioning plates present sixteen threaded M5 holes used to fix the two guides plus a central shoulder for the correct installation of the parts. Four supports guarantee the correct levelling of the structure.
- Joints: the structure of the universal joints of the real scale robot has been preserved.
- Links: Due to the dimensions of the links they are divided into two parts. The lower part contains a mechanism to allow the relative rotation of the two ends which is like the one of the real scale links. However, in this version a plug to keep the external parts of the bearings is needed. The upper part of the link is a simple cylindrical element.
- Platform: it is realized in a single component and six holes are drawn to install a smaller load cell. Specific planes are realized on the lateral surface of the platform so that the joints can be housed with the proper orientation specified by the optimization process.

Figure 4.20: Hexaslide scaled version

4.10 Purchased components

Following, the final choices regarding motors, linear actuators and the energy chain are listed.

4.10.1 Motors

The selected model is **the OMRON R88M-K2K030F-BS2** whose main characteristics are collected in Tab 4.1. The Lifting system motor, that must bear the torque increment given by the low efficiency of the trapezoidal screw adopted, is the **OMRON R88M-K20030T-BS2**, whose main characteristics are reported in Tab 4.2. Both motor models mount an auxiliary brake for safety reasons and an encoder to allow having the control of position and velocity. For the 2KW motor of the robot the encoder is a quadrature incremental encoder with a maximum resolution of 4194304cnt/rev.
The encoder signal is processed in order to obtain a lower resolution of 131072cnt/rev. The resulting linear resolution of 3276800cnt/m is obtained considering a lead of 0,04m/rev for the ball-screw linear axis. For the lifting system motor, the maximum encoder resolution is 131072cnt/rev. The modified used resolution is of 13107,2 cnt/rev, thus obtaining the same linear resolution of the robot's axis thanks to a smaller lead of 0.004m/rev.

Characteristic	Value	MU
Tension	400	V
Nominal Power	2000	W
Nominal Torque	6.37	Nm
Maximum Torque	19.1	Nm
Nominal velocity	3000	rpm
Maximum velocity	5000	rpm

Table 4.21: OMRON R88M-K2K030F-BS2 main characteristics

Characteristic	Value	MU
Tension	230	V
Nominal Power	200	W
Nominal Torque	0.64	Nm
Maximum Torque	1.91	Nm
Nominal velocity	3000	rpm
Maximum velocity	6000	rpm

Table 4.2: OMRON R88M-K20030T-BS2 main characteristics

4.10.2 Linear actuator

The linear actuator chosen is the model **TH145 SP4**, produced by **ROLLON** and whose characteristics are reported in Tab 4.3. The following customizations are required:

- Screw lead of 40mm per revolute, needed for the required performances
- Two calibrated centring holes on its lower side to correctly assembly the central plate
- Two calibrated centring holes on the external carriage allow the correct positioning of the Joint holder.

Characteristic	Value	MU
Total length	1100	mm
Width	145	mm
Thickness	85	m
Screw diameter	20	mm
Number of charts	2	–
Total system mass	~ 30	kg

Table 4.3: ROLLON TH145 SP4 main characteristics

4.10.3 Other components

The selected energy chain is **Igus Riflex TRE.40** whose main characteristics are reported in Tab 4.4.

Characteristic	Value	MU
Total length	1600	mm
Number of chain links	116	-
External diameter	43	mm
Curvature radius	58	mm
Maximum single cable diameter	13	mm
Maximum relative rotation	± 10	$^\circ$

Table 4.4: Igus Triflex TRE.40 main characteristics

Tapered roller bearings chosen both for the links and joints are the **INA FAG 30202-A**. They support both axial and radial loads avoiding the usage of more than one bearing. **KTR-TOOLFLEX20M** motor coupling is chosen.

Due to the reduced space available for the Lifting system, a more compact model of bearing **INA FAG 3000-B-2RS-TVH** is chosen. It is a double row angular contact ball bearing, that can support both axial and radial loads.
KTR Rotex 19/92Sh-A/2.1-Φ11/2.0-Φ8 motor coupling is chosen for the Lifting system and it provides required performances and encumbrance constraints.

4.11 Model analysis

In this section the approach followed to assess the correctness of the overall design, in terms of the overall dynamic behaviour, is reported. More specifically, the goal is to verify that the first natural frequency of the coupled structure, turbine mounted on the Hexaslide platform, coincides with the turbine first natural frequency, in order to be sure, the robot is not changing the turbine eigenfrequency and thus considering the presence of the robot negligible.
Nevertheless, the modal behaviour of a robot strongly depends on the specific pose of the end effector, since the mass and stiffness distribution vary consequently. It is beyond the scope of the present document to go into the details of this aspect, however normal modes and their associated frequencies are computed to merely verify that the frequency corresponding to the first normal mode was well above the required frequency range, regardless of the associated modal shape, for a set of chosen robot's poses.
The workspace has been discretized, and the trend of the frequency corresponding to the first normal mode all over the workspace has been mapped on specific planes that intersect the robot workspace. The procedure is listed below:

1. Identification of planes that intersect the workspace
2. Identification of a grid of equally spaced point on each plane
3. Discretization of pitch, roll and yaw angles describing the end-effector orientation:
    - Three roll angles: -5°, 0°, +5°
    - Five pitch angles: -8°, -4°, 0°, +4°, +8°
    - Three yaw angles: -3°, 0°, +3°
4. Modification of the pose of the robot in order to have the end-effector placed in correspondence of each point of the grid and exploring all the possible orientation.
5. In correspondence of each pose, linearization of the flexible virtual model and computation of the frequency associated to the first normal mode.
6. For each point of the grid, recording of the lowest value of frequency among the ones obtained by changing the orientation angles.

The result is a set of maps, one for each intersecting plane, which show the trend of the lowest frequencies regardless of the orientation of the robot.

4.11.1 Modal Analysis Results

A simplified structure is assembled in Inventor in order to reducing the computational cost but preserving the DoFs of the robot. Lower simplified joints are constrained to the ground applying spherical pins and the simulation provides the first three eigenmode frequencies. Links can be considered as the main cause for a possible worsening of the behaviour of the coupled system. The main deformations are concentrated on links and an advanced multibody model has been developed in ADAMS environment, whose links are made of two extremity elements and an intermediate one characterised by aluminium properties.
The results given by the two numerical environments are reported in Table 4. and Table 4.. For the sake of completeness, in Figure 4..

Eigenmode index	Frequency
I	151 Hz
II	154 Hz
III	210 Hz

Table 4.5: Eigenmodes frequencies in Home Position obtained in Inventor

Eigenmode index	Frequency
I	169 Hz
II	171 Hz
III	222 Hz

Table 4.6: Eigenmodes frequencies in Home Position obtained in Adams

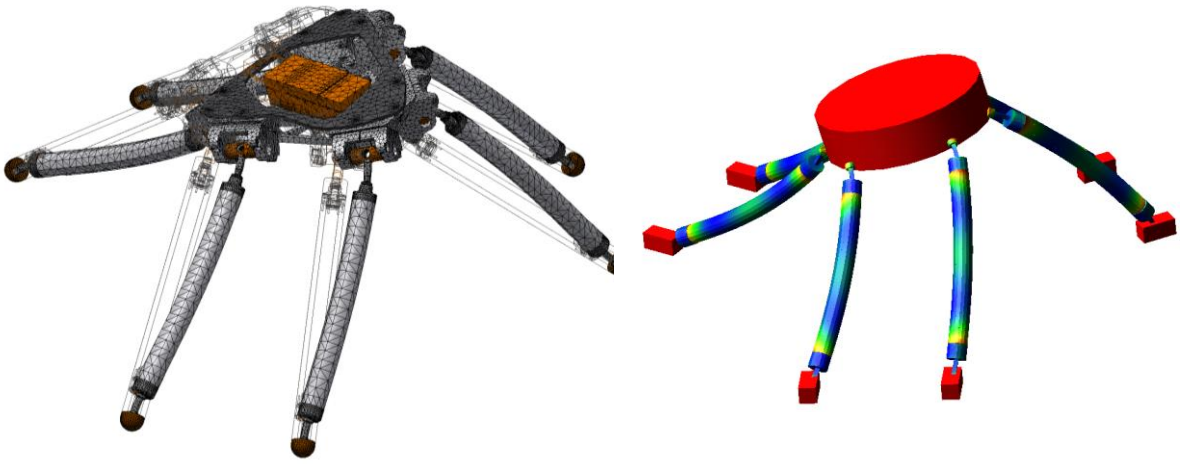

Figure 4.21 Numerical Modal Analysis

4.11.2 Experimental Verification

By the time of this document, the experimental verification of the dynamic response of the robot is currently being finalized. For the sake of completeness, the system, equipped with accelerometers, for the modal analysis campaign is shown in Figure 4.22. From the first rough results it has been confirmed that the robot will not interfere, from a dynamic point of view, with the wind turbine scale model [3].

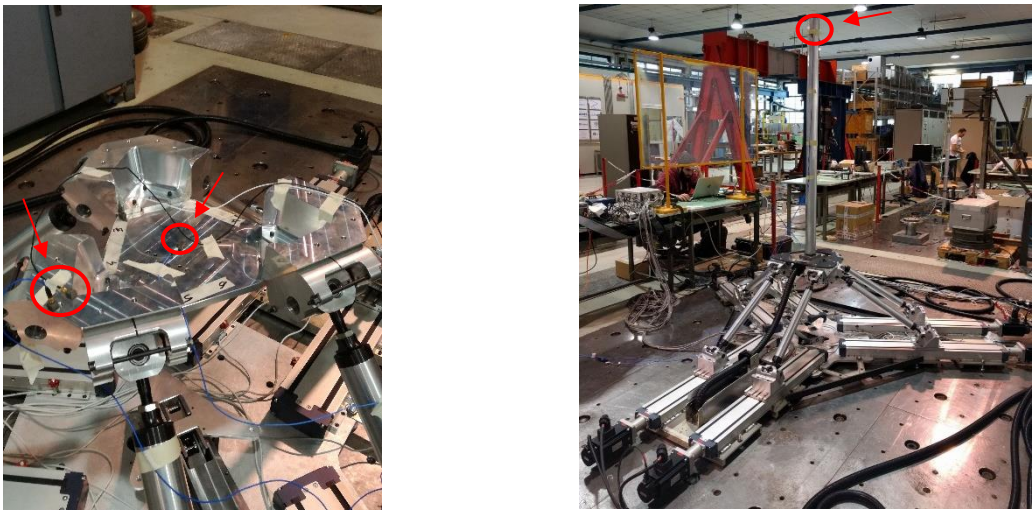

Figure 4.22: Hexafloat experimental modal analysis setup

5 Control architecture and electronics

A simplified scheme of the electric panel configuration is reported in Figure 5.1.
The core of the electrical panel is represented by Power PMAC, the controller property of Delta Tau Data Systems. There are essentially two zones: one with AC voltage, represented with the solid black and blue lines, that takes power from the 380 V AC line and brings it to the Power PMAC fed at 230 V and to the power circuits of the servo amplifiers fed at 380 V, and the other one with 24 V DC voltage, downstream of the 24 V power supply, that is represented by the solid and dashed green lines. This circuit provides power to the safety relay, to the limit switches and proximity sensors and to the Beckhoff modules for Ether-CAT communications. Red lines represent the transmission of data between different components.

EtherCAT modules: the Beckhoff EtherCAT module EK1100 is connected to two EL1008 modules, each of them providing 8 digital inputs, and to one EL2008 module that makes available 8 digital outputs.
Servo amplifiers: their main function is to properly power the motors according to the signals coming from the motion controller. They also process and gather the feedback signals of the motors encoders to bring them to the Power PMAC. Both the signals are transported to and from the servo amplifier into a single cable that is then split in a proper terminal board to be brought to the correct connectors of the Power PMAC. Each servo amplifier has the main task of closing the current and phase commutation feedback loop for the motor, starting from the torque reference provided by the Power PMAC motion controller.

Power PMAC: this is the core of the electrical architecture, it is a general-purpose embedded computer with a built-in motion and machine-control application. It also provides a wide variety of hardware machine interface circuitry that permits connection to common servo and stepper drives, feedback sensors, and analogue and digital I/O points.
The modular rack is the most flexible configuration since it permits the user to choose which CPU card, digital or analogue I/O card, axis interface cards, etc. to use in the system. The Power PMAC can handle all the tasks required for machine control, constantly switching back and forth between the different tasks thousands of times per second. On this powerful controller, the main control software of the robot is designed and implemented. The software architecture is structured so that a primary and a secondary state machine manage the logic state and functioning of the machine, managing exceptions, control mode specific routines start, stop and runtime checks, motion programs, safety routines and debug towards the user. The lowest level of the control is constituted by the position and velocity servo loops, giving the analogic torque output reference for the seven-servo actuator. Each high level control modality developed has been designed to respect real time performances desired and safety [14], using advanced tool like position based admittance control, buffering with time-base control, motion look-ahead for smooth blending, fast C written non-linear FK and demanding algebra, workspace boundaries check with controlled dynamics on the limits [15], acceleration saturation with workspace reference tracking check.
The Human-Machine-Interface (HMI) designed allow full control by the user of every significant functioning parameter, simplifying state change and enhancing safety. The HMI communicates with Power PMAC by means of Telnet communication protocol and is completely written in C# language. Full scale machine and the scaled prototype share the exact same control software, except for essential scale factors and hardware end electronics size and parameters.

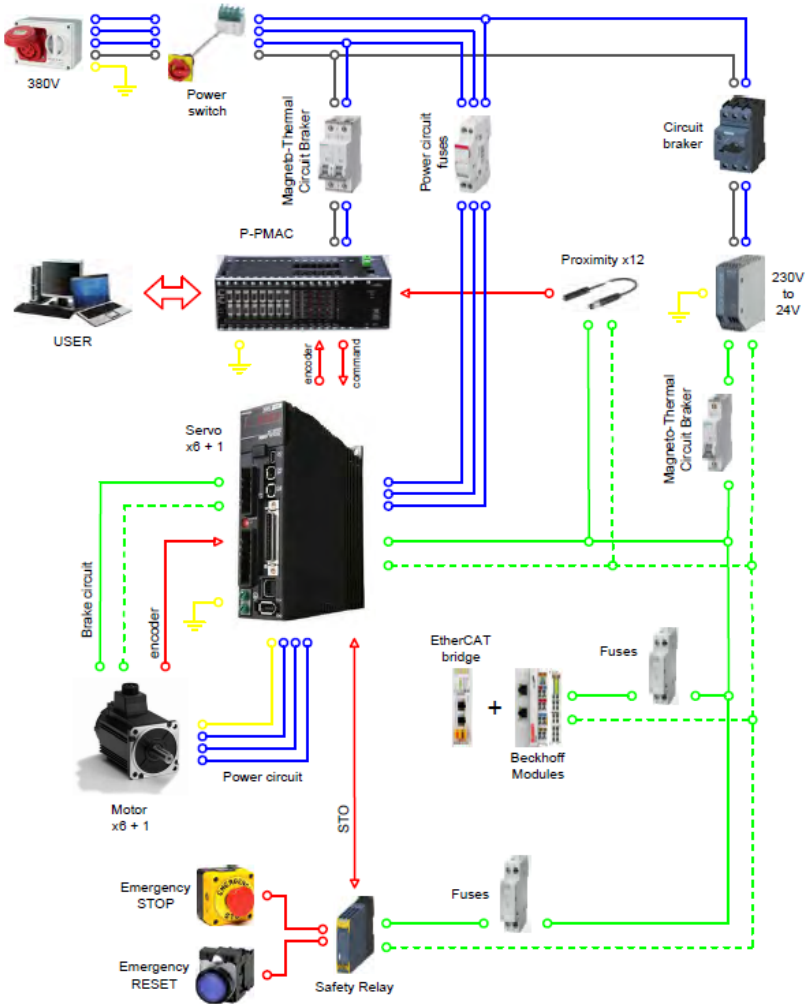

Figure 5.1: Simplified scheme of electrical layout

6 Conclusions

The present document reported the design methodology of the HexaFloat system, a 6-DoF robot for wind tunnel hybrid testing of floating offshore wind turbines. This setup consists in a parallel kinematic robot, “HexaFloat”, designed and developed by the authors of this report, to tests the dynamics of floating offshore wind turbine concepts, selected within LIFES50+ project, at Politecnico di Milano wind tunnel, through a hybrid methodology which combines, in real-time, measurements (i.e. aerodynamic forces on the wind turbine scale model) and computations (i.e. hydrodynamic forces on platform). This represents the complementary test approach, with respect to the one developed at SINTEF Ocean basin. The different chapters give the following information: Geometric optimization, Actuation chain sizing Mechanical design and sizing, Control architecture and electronics. By the time of this document the experimental verification of the design is currently being carried out, with promising results, confirming the correctness of the structured methodology herein reported.

7 References

[1] T. C. V. T. M. B. E. S. L. Sauder, "Real-time hybrid model testing of a braceless semi-submersible wind turbine. Part I: The hybrid approach," in *Proceedings of the International Conference on Offshore Mechanics and Arctic Engineering - OMAE*, 2016.

[2] M. B. D. F. F. F. H. G. I. Bayati, "Design of a 6-DoF Robotic Platform for Wind Tunnel Tests of Floating Wind Turbines," 2014, Energy Procedia.

[3] I. Bayati, M. Belloli, L. Bernini, H. Giberti and A. Zasso, "Scale model technology for floating offshore wind turbines," *IET Renewable Power Generation*, pp. DOI: 10.1049/iet-rpg.2016.0956 IET Digital Library, 2017.

[4] I. A. M. S. Ambrosini, "Methodological and technical aspects of a 2DoF/HIL setup for wind tunnel tests of floating systems," *Journal of Dynamic Systems, Measurement and Control*, 2018.

[5] M. B. A. F. I. Bayati, "Wind tunnel 2-DoF hybrid/HIL tests on the OC5 Floating Offshore Wind Turbine," *36th International Conference on Ocean, Offshore and Arctic Engineering, Trondheim (Norway)*, pp. OMAE2017-61763, 2017.

[6] L. B. M. B. A. Z. I. Bayati, "Aerodynamic design methodology for wind tunnel tests of wind turbine rotors," *Journal of Wind Engineering and Industrial Aerodynamics*, no. 10.1016/j.jweia.2017.05.004, June 2017.

[7] A. A. H. M. I.Bayati, "A novel wind tunnel/HIL setup for integrated tests of Floating Oshore Wind Turbines," in *The science of making torque from wind*, Milan, 2018.

[8] I. Bayati, M. Belloli, D. Ferrari, F. Fossati and H. Giberti, "Design of a 6-DoF robotic platform for wind tunnel tests of floating wind turbines.," *Energy Procedia*, no. 53, p. 313–323, 2014.

[9] H. Giberti and D. Ferrari, "A novel hardware-in-the-loop device for floating offshore wind turbines and sailing boats," *Mech. Mach. Theory*, no. 85, p. 82–105, 2015.

[10] E. Fiore and H. Giberti, "Optimization and Comparison between two 6-DoF Parallel Kinematic Machines for HIL Simulations in Wind Tunnel.," in *EDP Sciences*, Les Ulis, France, 2016.

[11] D. Ferrari and H. Giberti, "A genetic algorithm approach to the kinematic synthesis of a 6-DoF parallel manipulator.," in *2014 IEEE Conference on Control Applications (CCA)*, Juan Les Antibes, France, 2014.

[12] E. Fiore, H. Giberti and D. Ferrari, "Dynamics modeling and accuracy evaluation of a 6-DoF hexaslide robot.," in *Nonlinear Dynamics*, Berlin/Heidelberg, Germany, Springer, 2016, p. 473–479.

[13] H. Giberti and D. Ferrari, "Drive system sizing of a 6-DOF parallel robotic platform.," in *ASME 12th Biennial Conference on Engineering Systems Design and Analysis (ESDA 2014)*, Copenhagen, Denmark, 2014.

[14] F. La Mura, G. Todeschini and H. Giberti, “High Performance Motion-Planner Architecture for Hardware-In-the-Loop System Based on Position-Based-Admittance-Control.,” *Robotics MDPI,* vol. 7, no. 8, 2018.

[15] F. La Mura, P. Romanó, E. Fiore and H. Giberti, “Workspace Limiting Strategy for 6 DOF Force Controlled PKMs Manipulating High Inertia Objects.,” *Robotics MDPI,* vol. 7, no. 10, 2018.